

**PETROGRAPHY AND MINERALOGY  
OF THE MIOCENE ROCKS  
IN AGRUD AREA, NORTHWEST OF SUEZ, EGYPT**

**Presented by  
AHMED ABD EL MONEIM SHARAF EL DIN  
B.Sc. (Hons.)**

**THESIS  
Presented in Partial Fulfilment for the Requirements of the Degree of  
MASTER OF SCIENCE  
In  
GEOLOGY**

**GEOLOGY DEPARTMENT**

**FACULTY OF SCIENCE**

**AIN SHAMS UNIVERSITY**

**1992**

## APPROVAL SHEET

Title of Thesis: Petrography and mineralogy of the Miocene rocks in  
Agrud area, northwest of Suez, Egypt.

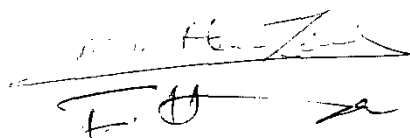
Thesis Advisors

APPROVED

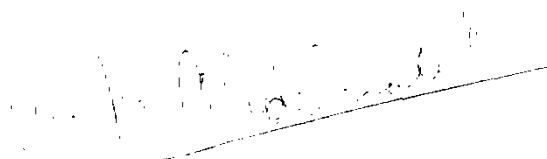
Prof. Dr. Mohamed Ezzeldin Hilmy

Prof. Dr. Mohamed M. Abu-Zeid

Dr. Fawzy H. Hamza



Prof. Dr. M.Y. Meneisy



Head of Geology Department



## N O T E

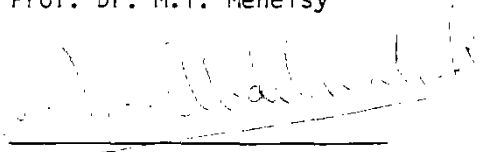
The present thesis is submitted to the Faculty of Science, Ain Shams University in partial fulfillment for the requirements of the degree of Master of Science in Geology.

Beside the research work materialized in this thesis, the candidate has attended the following ten post-graduate courses:

- 1- Field Geology and Mapping.
- 2- Laboratory Techniques.
- 3- Mineralogy.
- 4- Geochemistry.
- 5- Sedimentary Petrology.
- 6- Sedimentation.
- 7- Igneous Petrology.
- 8- Metamorphic Petrology.
- 9- Statistical Geology.
10. Ore Microscopy.

He has successfully passed the final examination of these courses, besides an English Language course.

Prof. Dr. M.Y. Meneisy



---

Head of Geology Department

### ACKNOWLEDGEMENT

I am deeply indebted to Prof. Mohamed Ezzeldin Hilmy (Professor of Mineralogy and Petrology), Prof. Mohamed M. Abu-Zeid (Professor of Sedimentary Rocks and Sedimentation) and Dr. Fawzy H. Hamza (Assistant Professor of Stratigraphy and Sedimentation) for their supervising the present research work, continuous help and sincere guidance during the various steps of fulfillment of this thesis. Special thanks are due to Prof. Mourad I. Youssef (Professor of Structural Geology) who suggested the point as an extension of previous stratigraphic and structural works.

I am grateful to Prof. M.A. Bassiouni (Dean of the Faculty of Science) and Prof. M.Y. Meneisy (Chairman of the Department of Geology) for the facilities and the financial aid from the University.

To all who cooperated in the progress of this work and in particular Prof. M. Boukhary, Prof. K.M. Amer (Earth Science Department, National Research Centre), Mr. A.R. Baghdady, Mr. M.E. El-Wakeel, Mr. H. Garamoon, Mr. Y.H. Dawood and Mr. A.M. Morsi. I offer my sincere thanks.

## TABLE OF CONTENTS

	Page
TABLE OF CONTENTS	i
LIST OF FIGURES	iii
LIST OF TABLES	x
 CHAPTER I - INTRODUCTION	
1.1 Distribution of the Miocene Rocks in Egypt	1
1.2 Previous Work on the Miocene Rocks in the Cairo-Suez District	3
1.3 Aim of the Work	11
 CHAPTER II - GENERAL GEOLOGY AND LITHOSTRATIGRAPHY	
2.1 General Geology	12
2.2 Lithostratigraphy	15
 CHAPTER III - PETROGRAPHY OF CLASTIC ROCKS	
3.1 Thin-Section Examination	38
3.2 Acid-Insoluble Residues	41
3.3 Particle-Size Distribution	49
 CHAPTER IV - MINERALOGY OF CLASTIC ROCKS	
4.1 Mineralogy of the Arenaceous Rocks	89
4.1.1 Mineralogy of the Light Fractions	89
4.1.2 Mineralogy of the Heavy Fractions	93
4.2 Mineralogy of the Argillaceous Rocks	110
4.2.1 The Nonclay Mineral Assemblage	111
4.2.2 The Clay Mineral Assemblage	116
 CHAPTER V - PETROGRAPHY AND PALEOECOLOGY OF CARBONATES (Microfacies Associations)	131
 CHAPTER VI - PETROGENESIS AND ENVIRONMENT OF DEPOSITION	
6.1 Petrogenesis	149
6.2 Environment of Deposition	152

	<b>Page</b>
CHAPTER VII - DIAGENESIS	
7.1 Diagenesis of Clastic Rocks	155
7.2 Diagenesis of Nonclastic Rocks	158
SUMMARY AND CONCLUSION	162
REFERENCES	173
ARABIC SUMMARY	-

## LIST OF FIGURES

	Page
Fig. (1.1) Distribution of the Miocene outcrops in Egypt (simplified after Geological Survey of Egypt, 1981).	2
Fig. (2.1) Location Map of the study area, Cairo-Seuz Railway	13
Fig. (2.2) Topography Map of the Agrud area showing location of the studied sections (modified after HAMAM, (1966)).	14
Fig. (2.3) Stratigraphic columnar section of the Oligocene and Miocene sequences in section I.	22
Fig. (2.4) Stratigraphic columnar section of the Miocene sequence in section II.	26
Fig. (2.5) Stratigraphic columnar section of the Miocene sequence in section III.	26
Fig. (2.6) Stratigraphic relationships of the studied sequences.	28
Fig. (2.7) Composite stratigraphic columnar section of the Oligocene and Miocene sequences in Agrud area.	29
Fig. (2.8) A general view of the lower and middle parts of the Oligocene sand section (section I).	30
Fig. (2.9) A general view of the middle part of the Oligocene Section. The base shows a rapid lateral variation from white sand (right) to brown pebbles and gravels (left) (section I).	30
Fig. (2.10) A general view of the middle and upper parts of the Oligocene section. The middle part is completely covered by loose sands (section I).	30
Fig. (2.11) A close up of the topmost part of the Oligocene section. The soil zone (S) is composed of sandy argillaceous sediments which are stained with red and brown iron oxides and contain molds of plant roots and stems in life position (section I).	31
Fig. (2.12) The Oligocene-Miocene contact. The Oligocene sands are overlain by a light grey mudstone layer and followed by the <i>Scutella</i> sandy limestone bed, both are of Miocene age. (section I).	31
Fig. (2.13) A general view of the lower part of the Miocene rock unit M <sub>1</sub> . The sequence is capped by the first algal limestone bed (section I).	31
Fig. (2.14) A general view of the upper part of the Miocene rock unit M <sub>1</sub> . The sequence is capped by a thick oyster limestone bed which forms the base of the Miocene rock unit M <sub>2</sub> (section I).	32



Fig. (2.15)	A general view of the contact between the rock units M <sub>2</sub> and M <sub>3</sub> (section III).	32
Fig. (2.16)	A close up of the lower part of the Miocene rock unit M <sub>3</sub> which is formed of white jointed limestones (section III).	32
Fig. (2.17)	An exposure (quarry face) of the limestones which form the Miocene rock unit M <sub>3</sub> (section III).	33
Fig. (2.18)	Thinly-bedded limestones in the topmost part of the Miocene rock unit M <sub>3</sub> (section III).	33
Fig. (2.19)	Tabular, high angle cross-bedding in the Oligocene fine-grained sandstones (section I).	33
Fig. (2.20)	Trough cross-bedding and colour lamination in the Oligocene fine- to medium-grained sandstones (section I).	34
Fig. (2.21)	Wedge shaped cross-bedding, colour lamination and graded-bedding in the Oligocene pebbly sandstone. The bed contains a thin conglomeratic band (section I).	34
Fig. (2.22)	Channelling and colour lamination in the Oligocene fine- to medium-grained pebbly sandstones (section I).	34
Fig. (2.23)	Colour lamination and small-scale corss-bedding (top left) in the Oligocene pebbly fine- to medium-grained sandstone. The strata are affected by a minor normal fault (F) (section I).	35
Fig. (2.24)	Bands and lenses of iron and manganeze oxides in the Oligocene coarse-grained sandstone (section I).	35
Fig. (2.25)	Hard, carbonate-cemented sandstone bodies in the middle and upper parts of the Oligocene section. These bodies were most probably diagenetically formed (section I).	35
Fig. (2.26)	Cavernous limestone in the middle part of the Miocene rock unit M <sub>3</sub> . The vugs were probably the results of diagenetic solution (section III).	36
Fig. (2.27)	A large number of <i>Scutella</i> sp. tests in the sandy limestone which forms the base of the Miocene rock unit M <sub>1</sub> (section I)	36
Fig. (2.28)	A pectinid-bryozoan shells bed overlain by a fractured, algal limestone layer in the lower part of the Miocene rock unit M <sub>1</sub> (section I).	36
Fig. (2.29)	Calcareous sandstone with abundant shell of <i>Pecten josslingi</i> in the upper part of the Miocene rock unit M <sub>1</sub> (section I).	37
Fig. (2.30)	Calcareous sandstone with tests of <i>Scutella</i> sp. in the top of the Miocene rock unit M <sub>1</sub> (section I).	37
Fig. (3.1)	Calcareous quartz arenite. Quartz grains are medium to coarse sand-sized, moderately-sorted and subangular to subrounded. The matrix is made up of sparry calcite (sample 66, rock unit M <sub>2</sub> , crossed polars, X 40).	42

- Fig. (3.2) Calcareous quartz arenite. The rock is composed of fine sand-sized quartz grains and chert fragments. The remarkable sorting of the detrital grains suggests a multi-cyclic origin (sample 10, Oligocene, crossed polars, X 100). 42
- Fig. (3.3) Calcareous pebbly sandstone. The photomicrograph shows parts of monocrystalline (m) and polycrystalline (p) pebbles. The marked corrosion and etching of the latter grains by calcite (arrows) suggests a relatively lower stability. (sample 48, rock unit M<sub>1</sub>, crossed polars, X 100). 42
- Fig. (3.4) Fossiliferous calcareous sandstone. recrystallized fossil shells (?) and detrital quartz and glauconite (g) grains are embedded in a sparitic matrix. (sample 48, rock unit M<sub>1</sub>, plane-polarized light, X 100). 43
- Fig. (3.5) A markedly rounded monocrystalline quartz grain showing eroded overgrowths (arrows) indicate of recycling. (sample 69, rock unit M<sub>2</sub>, crossed polars, X 100). 43
- Fig. (3.6) Allochthonous glauconite in calcareous sandstone. The carbonates of the matrix are made up mainly of small, zoned rhombohedra of dolomite. (sample 43, rock unit M<sub>1</sub>, plane-polarized light, X 100). 43
- Fig. (3.7) Partly oxidized allochthonous glauconite in calcareous sandstone. Oxidation to hematite was more profound along the cracks that were developed earlier probably due to dehydration as a result of compaction. (sample 66, rock unit M<sub>2</sub>, plane-polarized light, X 100). 44
- Fig. (3.8) Embayment of a monocrystalline quartz grain by sparitic calcite of the rock matrix (arrows). Corrosion of the grains probably accompanied recrystallization of an original micrite (sample 51, rock unit M<sub>1</sub>, crossed polars, X 100). 44
- Fig. (3.9) Invasion and replacement of a polycrystalline quartz pebble by calcite. Remnants of the original quartz grain (r) are seen (sample 53, rock unit M<sub>1</sub>, crossed polars, X 100). 44
- Fig. (3.10) Replacement of sparry calcite (c) by microcrystalline silica (s). This diagenetic process most probably followed corrosion of quartz grains (arrows) by the sparitic calcite (sample 72, rock unit M<sub>2</sub>, crossed polars, X 100). 45
- Fig. (3.11) Sandy limestone. Rounded, coarse sand-sized quartz grains are embedded in a matrix of sparry calcite. (sample 59, rock unit M<sub>2</sub>, plane-polarized light, X 100). 45
- Fig. (3.12) Gypsiferous sandy limestone. The original micritic calcite of the rock matrix (c) has been replaced by fibrous gypsum (g). (sample 40, rock unit M<sub>1</sub>, crossed polars, X 100). 45
- Fig. (3.13) Percentage-constituent of the acid-insoluble residues in the Miocene sequence. 47
- Fig. (3.14) Nomenclature of the studied carbonates based on the scheme proposed by FÜCHTBAUER and MÜLLER (1970). 53

Fig. (3.15)	Nomenclature of the Oligocene and Miocene clastic sediments based on the scheme proposed by PICARD (1971).	53
Fig. (3.16)	Vertical variation in the composition of the studied sediments.	55
Fig. (3.17)	Vertical variation in the proportions of grain-size classes in the studied section.	56
Fig. (3.18)	Histograms showing the distribution of particle sizes in the Oligocene arenaceous sediments.	59
Fig. (3.19)	Histograms showing the distribution of particle sizes in the Miocene (M <sub>1</sub> ) arenaceous sediments.	60
Fig. (3.20)	Histograms showing the distribution of particle sizes in the Miocene (M <sub>2</sub> ) arenaceous sediments.	61
Fig. (3.21)	Histograms showing the distribution of particle sizes in the argillaceous sediments of the Miocene rock unit M <sub>1</sub> .	62
Fig. (3.22)	Histograms showing the distribution of particle sizes in the argillaceous sediments of the Miocene rock unit M <sub>2</sub> .	63
Fig. (3.23)	Cumulative curves of the Oligocene sand samples.	64
Fig. (3.24)	Cumulative curves of the Miocene (M <sub>1</sub> ) sand samples.	65
Fig. (3.25)	Cumulative curves of the Miocene (M <sub>2</sub> ) sand samples.	66
Fig. (3.26)	Frequency distribution of the arenaceous samples among the various mean size classes.	74
Fig. (3.27)	Frequency distribution of the arenaceous samples among the various sorting classes.	74
Fig. (3.28)	Frequency distribution of the arenaceous samples among the various skewness classes.	77
Fig. (3.29)	Frequency distribution of the arenaceous samples among the various kurtosis classes.	77
Fig. (3.30)	Cumulative curves of the Miocene (M <sub>1</sub> ) argillaceous samples.	79
Fig. (3.31)	Cumulative curves of the Miocene (M <sub>2</sub> ) argillaceous samples.	80
Fig. (3.32)	Frequency distribution of the arenaceous samples among the various mean size classes.	83
Fig. (3.33)	Plots of standard deviation vs. mean size for the sand samples (diagram after MOIOLA and WEISER, 1968).	84
Fig. (3.34)	Plots of skewness vs. mean size for the sand samples (diagram after MOIOLA and WEISER, 1968).	84

	Page
Fig. (3.35) Plots of skewness vs. standard deviation for the sand samples (diagram after FRIEDMAN, 1967).	86
Fig. (3.36) Plots of first percentile vs. standard deviation for the sand samples (diagram proposed by FRIEDMAN, 1967).	86
Fig. (3.37) Plots of the sand samples on the C-M pattern proposed by PASSEGA and BRYAMJEE (1969).	88
Fig. (3.38) Plot of the Miocene argillaceous samples on the C-M pattern proposed by PASSEGA and BYRAMJEE (1969).	88
Fig. (4.1) Vertical variation of heavy index. ZTR index and percentages of opaques in the studied sequence.	96
Fig. (4.2) Frequency distribution of non opaque minerals in the studied sequence.	98
Fig. (4.3) A photomicrograph showing a rounded grain of brown tourmaline (t) together with more angular grains of kyanite (k), epidote (e) and staurolite (st). (sample 48, rock unit M <sub>1</sub> , fine sand fraction, X 40).	104
Fig. (4.4) A photomicrograph showing grains of rutile (r), garnets (g), epidote (e) and hornblende (h). (sample 72, rock unit M <sub>1</sub> , fine sand fraction, X 40).	104
Fig. (4.5) A photomicrograph showing grains of hornblende (h), epidote (e) and euhedral and rounded zircon (z) grains. (sample 69, rock unit M <sub>2</sub> , fine sand fraction, X 40).	105
Fig. (4.6) A photomicrograph showing grains of tourmaline (t), epidote (e), garnet (g), zircon (z) and kyanite (k). (sample 21, rock unit M <sub>1</sub> , fine sand fraction, X 40).	105
Fig. (4.7) X-Ray diffraction patterns of the bulk samples from the argillaceous rocks in the Miocene rock unit M <sub>1</sub> .	112
Fig. (4.8) X-Ray diffraction patterns of the bulk samples from the argillaceous rocks in the Miocene rock unit M <sub>2</sub> .	113
Fig. (4.9) X-Ray diffraction patterns of the clay fractions from the argillaceous rocks in the Miocene rock unit M <sub>1</sub> .	117
Fig. (4.10) X-Ray diffraction patterns of the clay fractions from the argillaceous rocks in the Miocene rock unit M <sub>2</sub> .	119
Fig. (4.11) Vertical distribution of the clay minerals in the Miocene sequence.	124
Fig. (5.1) Facies scheme after WILSON (1975). Sequence of the Standard Microfacies Type.	132
Fig. (5.2) Sandy echinid biomicrite. The micrite matrix is highly ferruginous (sample 17, rock unit M <sub>1</sub> , crossed polars X 40).	143

Fig. (5.3)	Microfacies type as above, note the presence of <i>Miogypsina</i> sp. (sample 17, rock unit M <sub>1</sub> , plane-polarized light, X 40).	143
Fig. (5.4)	Sandy molluscan foraminiferal biomicrite. Note the presence of neomorphic microsparite in the micritic groundmass (sample 35, rock unit M <sub>1</sub> , plane-polarized light, X 40).	143
Fig. (5.5)	Sandy biosparite (carbonate 54%) with foraminiferal skeletal grains (sample 22, rock unit M <sub>1</sub> , plane-polarized light, X 40).	144
Fig. (5.6)	Sandy molluscan biosparite, note fractured molluscan shell fragments; cracking and oxidation of the irregular glauconitic grains to dark brown iron oxide (sample 40, rock unit M <sub>1</sub> , crossed polars, X 40).	144
Fig. (5.7)	Microfacies as above. A part of <i>Miogypsina</i> sp. test, its chambers are filled either with sparitic calcite or micritic materials (sample 40, rock unit M <sub>1</sub> , plane-polarized, X 40).	144
Fig. (5.8)	Foraminiferal algal biolithite, note the presence of spar-filled holes (conceptacles) in the algal fragment (h) (sample 29, rock unit M <sub>1</sub> , crossed polars, X 40).	145
Fig. (5.9)	Microfacies type as above, note the algal voids filled with brownish micrite (sample 29, rock unit M <sub>1</sub> , plane-polarized light, X 40).	145
Fig. (5.10)	Algal molluscan biomicrite, note the partial micritization of the molluscan shell fragments (sample 56, rock unit M <sub>2</sub> , plane-polarized light, X 40).	145
Fig. (5.11)	Foraminiferal algal biomicrite (sample 58, rock unit M <sub>2</sub> , plane-polarized light, X 40).	146
Fig. (5.12)	Algal biolithite, the algal mats are outlined by their micrite periphery (sample 57, rock unit M <sub>2</sub> , plane-polarized light, X 40).	146
Fig. (5.13)	Sandy biosparite with benthonic foraminiferal tests (sample 60, rock unit M <sub>2</sub> , Plane-polarized light, X 132).	146
Fig. (5.14)	Sandy algal biosparite showing dark brownish colored (by iron oxides) micrite envelope (sample 75, rock unit M <sub>2</sub> , crossed polars, X 40).	147
Fig. (5.15)	Sandy molluscan foraminiferal biosparite voids of the foraminiferal test ( <i>Amphestigina</i> sp.) are filled with ferruginous micrite (sample 66, in section I, rock unit M <sub>2</sub> , crossed polars, X 40).	147
Fig. (5.16)	Sandy biomicrite (sample 63, rock unit M <sub>2</sub> , plane-polarized light, X 40).	147

- Fig. (5.17) Algal biosparite, note the highly calcareous of the foraminiferal test (*Amphestigina* sp.) on the right hand (sample 85, rock unit M<sub>3</sub>, plane-polarized light, X 40). 148
- Fig. (5.18) Microfacies type as above, note the highly obliteration of the algal fragments (A) and the echinid fragments (E), and the presence of few foraminiferal tests (sample 87, rock unit M<sub>3</sub>, crossed polars, X 40). 148
- Fig. (5.19) Sandy molluscan foraminiferal biomicrite, note the diagenetic cementation represented by the precipitation of sparitic calcite filling the fracture in the molluscan shell fragment and the voids in the groundmass (sample 81, rock unit M<sub>3</sub>, plane-polarized light, X 40). 148

## LIST OF TABLES

	Page
Table (1.1) The different rock units of the marine Miocene in the Cairo-Suez-Sadat stretch as proposed by different authors (modified after EL GAMAL, 1971)	9
Table (3.1) Composition of the acid-insoluble residues of the Miocene carbonate rocks	46
Table (3.2) Composition and nomenclature of the studied Oligocene and Miocene sediments	51
Table (3.3) Characteristics of the cumulative curves of the studied arenaceous sediments and their possible depositional processes according to VISHNER (1969).	68
Table (3.4) Calculated particle-size parameters of the studied arenaceous sediments	71
Table (3.5) Frequency distribution of arenaceous samples among the various mean size classes.	73
Table (3.6) Frequency distribution of arenaceous samples among the various sorting classes	73
Table (3.7) Frequency distribution of the arenaceous samples among the various skewness classes	76
Table (3.8) Frequency distribution of the arenaceous samples among the various kurtosis classes	76
Table (3.9) Calculated particle-size parameters for the studied argillaceous sediments	82
Table (3.10) Frequency distribution of the argillaceous samples among the various mean size classes	83
Table (4.1) Distribution of various types of quartz in the Oligocene and Miocene arenaceous sediments	91
Table (4.2) Composition of the light fractions of the Oligocene and Miocene sands	94
Table (4.3) Frequency distribution of the non-opaque heavy minerals in the Oligocene and Miocene arenaceous sediments	97
Table (4.4) Average percentages of heavy-mineral species, heavy index and ZTR index in the arenaceous sediments	99
Table ((4.5) Values of ZTR index and number of non-opaque, nonmicaceous heavy minerals in the arenaceous sediments	109
Table (4.6) X-Ray diffraction data of bulk samples from the Miocene rock unit (M <sub>1</sub> )	114